JMEPEG (2011) 20:712–718
DOI: 10.1007/s11665-011-9838-y

1059-9495/$19.00

Theoretical and Experimental Study of the Shape Memory Effect of Beams in Bending Conditions

Ferdinando Auricchio, Simone Morganti, Alessandro Reali, and Marco Urbano

(Submitted June 8, 2010; in revised form November 5, 2011)

In this study, the shape memory effect of SMA beams under complex stress conditions is studied by means of a finite element model. The 1D version of a well-established SMA constitutive model is utilized in the numerical computations and the required parameters are obtained experimentally starting from thermal cycling tests in tension under different constant loads. After being calibrated, the model is used to compute the deformation of beams loaded in bending and undergoing thermal cycling; three-point bending and cantilever configurations are considered in this stage. Finally, the response predicted by the model is compared to experimental results and model capabilities are discussed. In particular, insight of the stress and strain evolution in bending is provided.

Keywords bending tests, numerical modeling, shape memory alloys

1. Introduction

Shape memory alloys (SMA) are materials exhibiting two functional properties: superelasticity and shape-memory effect. These properties are associated with a phase transformation from twinned martensite to austenite or from detwinned martensite to twinned martensite. While devices exploiting superelasticity have been widely employed for years—stents are the most interesting examples—only recently the application of the shape memory effect has grown from an embryonic state. One of the reasons for the late popularity of the shape memory effect has to be ascribed to the need of a thorough knowledge of the material for a proper design. Modeling could be an interesting mean for supporting engineers in the exploitation of the shape memory effect. Despite the availability of many models able to describe the SMA macroscopic effects (e.g., see Ref 1 and references therein), these can be hardly utilized by designers due to the difficulty of the calibration process. Moreover, model development has been often carried out with poor attention to experimental data and thus the potential user has little information about the real performances of a model. Only recently, activities with thorough comparisons between models and experimental data are being proposed (Ref 2).

This article is an invited paper selected from presentations at Shape Memory and Superelastic Technologies 2010, held May 16-20, 2010, in Pacific Grove, California, and has been expanded from the original presentation.

Ferdinando Auricchio, Simone Morganti, and **Alessandro Reali**, Dipartimento di Meccanica Strutturale, Università Degli Studi di Pavia, Pavia, Italy; and **Marco Urbano**, SAES Getters Group, Lainate, MI, Italy. Contact e-mails: ferdinando.auricchio@unipv.it, simone.morganti@unipv.it, alessandro.reali@unipv.it, and marco_urbano@saes-group.com.

A research program, aiming at assessing the performances and further developing the model proposed in Ref 3-5, is currently being carried out. The purpose of the study is also to identify reliable procedures for the model calibration. In this article, the shape memory effect of SMA beams under complex stress conditions is studied by means of a finite element (FE) model. In particular, the behavior of a cantilever beam predicted by the model is compared to experimental results. On this basis, model capabilities are discussed and insight of the stress and strain evolution in bending is provided.

2. Model Description

Like in other SMA models, the constitutive equations of the considered model are derived from the definition of a thermodynamic potential. Normally, the internal variable defining the phase transformation is the fraction of the product phase. Here, the transformation strain tensor (scalar in the 1D case) is chosen as internal variable. This choice poses some limitations, but many advantages, like the possibility of easily describing the martensite reorientation, and a corresponding simple and robust implementation.

Following (Ref 3-5), the free energy density function for the 1D case is defined as follows:

$$\psi(\varepsilon, \varepsilon^{tr}, T) = \frac{1}{2}E(\varepsilon - \varepsilon^{tr})^2 + \tau_m(T)\left|\varepsilon^{tr}\right|_2 + \frac{1}{2}h\left|\varepsilon^{tr}\right|_3^2 \mathcal{I}_{\varepsilon_L}\left(\left|\varepsilon^{tr}\right|_1\right) \quad \text{(Eq 1)}$$

where

$$\mathcal{I}_{\varepsilon_L}\left(\left|\varepsilon^{tr}\right|_1\right) = \begin{cases} 0 & \text{if } |\varepsilon^{tr}|_1 \leq \varepsilon_L \\ +\infty & \text{otherwise} \end{cases}$$

$$\left|\varepsilon^{tr}\right|_i = \sqrt{\varepsilon^{tr^2} + \delta} - c_i\varepsilon^{tr} \quad \text{(Eq 2)}$$

$$\tau_m(T) = \begin{cases} \beta(T - T^*) & \text{if } T > T^* \\ 0 & \text{otherwise} \end{cases}.$$

According to (1), the free energy density function is obtained as the sum of four terms, i.e., respectively, the standard elastic energy; the chemical energy, accounting for the thermally induced transformation; the mixing energy, accounting for the mixing build-up during the phase transformation. The last term, constituted by the indicator function, $\mathcal{I}_{\varepsilon_L}$, is a mathematical tool introduced to satisfy the transformation strain constraint:

$$\left|\varepsilon^{tr}\right|_1 \leq \varepsilon_L$$

It is worth noting that we assume as initial condition that the internal variable, i.e., the transformation strain, is equal to zero. This means that the material starts in its parent phase, i.e., for low temperatures, the twinned martensite phase.

Equation 1 and 2 are defined by the following parameters:

- E is the elastic modulus which is assumed to be identical for austenite and martensite;
- ε_L is the maximum transformation strain in tension;
- h is the stress-strain slope measure during transformation. This parameter accounts for the build-up of mixing energy during the phase transformation and is responsible for the slope of the ε-T loop and the σ-ε loop;
- β is the inverse of the variation of transformation temperatures with respect to stress during thermal cycling at constant load;
- T^* is the reference temperature;
- c_i is the three parameters describing the difference of behavior in tension and in compression;
- δ is a user-defined regularization parameter (typical value: 10^{-8}) that has been introduced so that the norm of the transformation strain is always differentiable.

The constitutive equations for the model are obtained by differentiating the free energy density function with respect to control and internal variables, as follows:

$$\sigma = \frac{\partial \psi}{\partial \varepsilon} = E(\varepsilon - \varepsilon^{tr}) \qquad \text{(Eq 3)}$$

$$X = -\frac{\partial \psi}{\partial \varepsilon^{tr}} = \sigma - \tau_m(T)\frac{\partial |\varepsilon^{tr}|_2}{\partial \varepsilon^{tr}} - h\left|\varepsilon^{tr}\right|_3 \frac{\partial |\varepsilon^{tr}|_3}{\partial \varepsilon^{tr}} - \gamma \frac{\partial |\varepsilon^{tr}|_1}{\partial \varepsilon^{tr}},$$

where X is the thermodynamic force associated to the transformation strain ε^{tr}. The variable γ derives from the subdifferential of the indicator function $\mathcal{I}_{\varepsilon_L}$ and is such that

$$\begin{cases} \gamma = 0 & \text{if } |\varepsilon^{tr}|_1 < \varepsilon_L \\ \gamma > 0 & \text{if } |\varepsilon^{tr}|_1 = \varepsilon_L \end{cases}.$$

To control the evolution of the internal variable ε^{tr}, a limit function F is introduced and is defined as

$$F(X) = |X| - R(T),$$

where the radius of the elastic domain $R(T)$ controls the width of the hysteresis loops. The dependence of R on the temperature T is shown in Fig. 1.

Considering an associative framework, the flow rule for the internal variable takes the form:

$$\dot{\varepsilon}^{tr} = \dot{\gamma}\frac{\partial F}{\partial X} = \dot{\gamma}\frac{X}{|X|}.$$

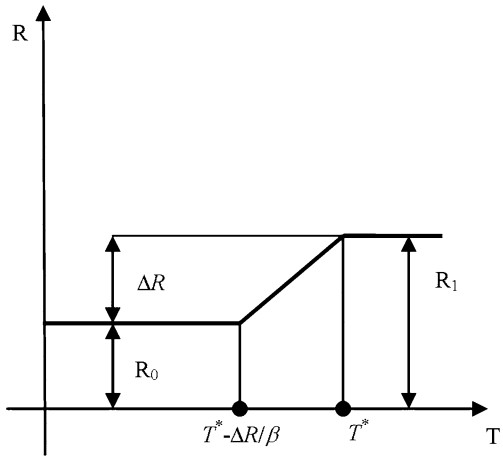

Fig. 1 Temperature dependence for the elastic domain radius R

The constitutive model is finally completed by the classical Kuhn-Tucker conditions:

$$\begin{cases} \dot{\gamma} \geq 0 \\ F \leq 0 \\ \dot{\gamma} F = 0 \end{cases}$$

Moreover, since we use only a single internal variable to describe phase transformations, at most it is possible to distinguish between a generic parent phase (not associated to any macroscopic strain) and a generic product phase (associated to a macroscopic strain). Accordingly, the model does not distinguish between the austenite and the twinned martensite, as both these phases do not produce macroscopic strain. For this reason, the radius R_0 depicted in Fig. 1 represents either the detwinning stress or the minimum stress at which the stress-induced transformation from austenite to detwinned martensite takes place. These two stresses are in general different in real materials.

3. Difference of Model Response in Tension and Compression

As anticipated in the previous section, the behavior difference in tension and compression is governed by means of the three parameters c_1, c_2, and c_3.

The first parameter, c_1, regulates the difference between the maximum transformation strains in tension and compression in a σ-ε loop or the different stroke during a ε-T loop. The effect of c_1 is shown in Fig. 2.

The second parameter, c_2, regulates the difference between the yield stress in tension and compression or, accordingly, the difference of transformation temperatures in a temperature loop at constant load. The effect of c_2 is shown in Fig. 3. The forward transformation stresses in tension and compression are, respectively:

$$\sigma_{yt} = \beta(T - T^*)(1 + c_2) + R(T)$$
$$\sigma_{yc} = -\beta(T - T^*)(1 + c_2) - R(T)$$

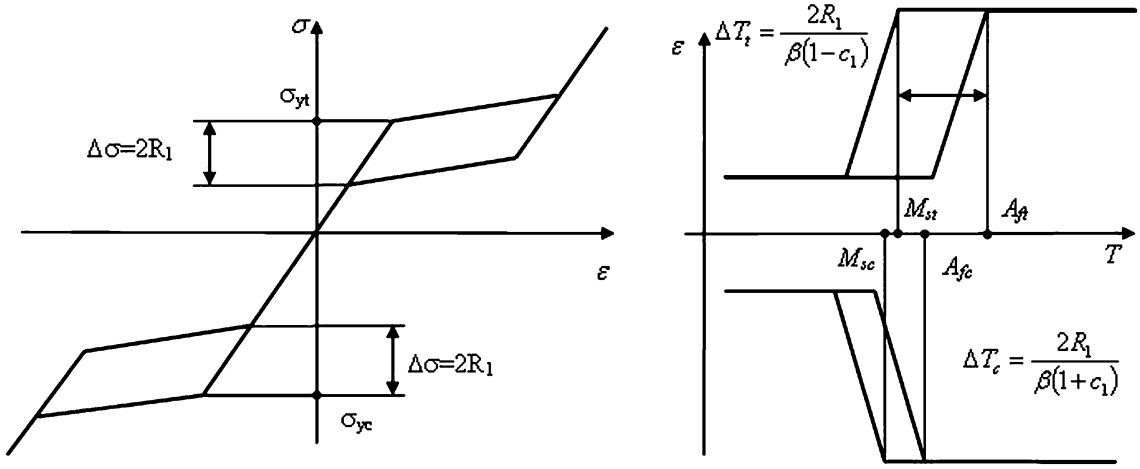

Fig. 2 Effect of the parameter c_1 in a typical stress-strain loop (left) and strain-temperature loop (right)

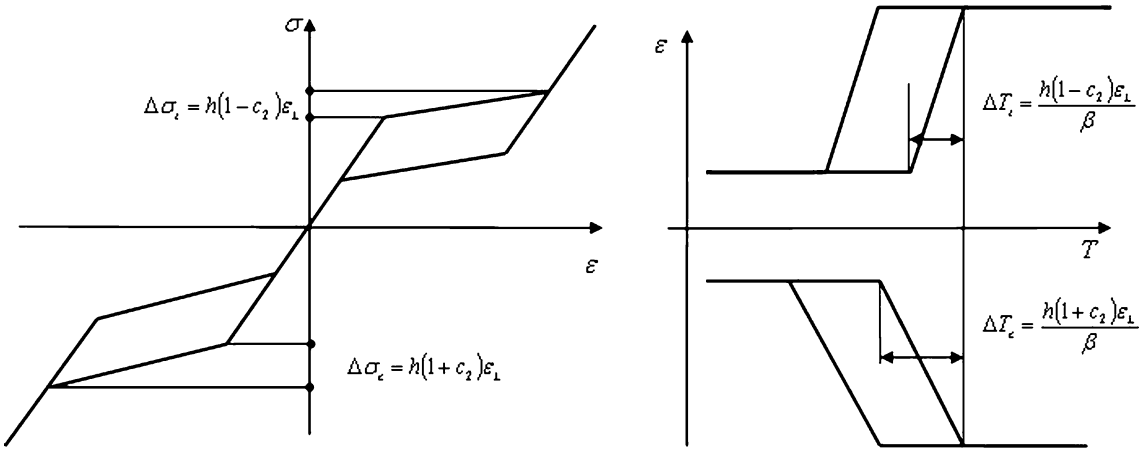

Fig. 3 Effect of the parameter c_2 in a typical stress-strain loop (left) and strain-temperature loop (right)

The martensite start and austenite finish temperatures in tension and compression are:

$$M_{st} = \frac{\sigma - R_1}{\beta(1 - c_2)} + T^*,$$
$$A_{ft} = \frac{\sigma + R_1}{\beta(1 - c_2)} + T^*,$$
$$M_{sc} = \frac{-\sigma - R_1}{\beta(1 + c_2)} + T^*,$$
$$A_{fc} = \frac{-\sigma + R_1}{\beta(1 + c_2)} + T^*$$

The third parameter, c_3, regulates the difference between the plateau slopes in tension and compression in a σ-ε loop or the difference between the transformation slopes during a ε-T loop. The effect of c_3 is shown in Fig. 4.

In this study, we choose the three parameters c_1, c_2, and c_3 to be independent: in particular we focus on the case $c_2 = c_3 = 0$ and $c_1 \geq 0$.

4. Parameter Identification from a ε-T Test

The method for deriving the model parameters in tension from experimental data is widely described in Ref 1. Two ε-T tests at two different constant stresses are needed (see Fig. 5).

Experimental testing has been performed on 0.5-mm high transformation temperature wires produced by SAES Getters. Temperature cycles under constant tension have been performed in a Weiss WK11-600 climatic chamber as described in Ref 7. The displacement versus temperature evolution has been measured for tensile loads of 100 and 50 MPa.

The maximum transformation strain in tension can be immediately obtained by measuring the stroke of the hysteresis loop at 100 MPa. The elastic modulus E and β can be derived as $E = \Delta\sigma/\Delta\varepsilon$ and $\beta = \Delta\sigma/\Delta T$, where the meaning of $\Delta\varepsilon$ and ΔT is indicated in Fig. 5; h can be instead obtained from

$$h = \frac{1}{\frac{1}{\beta\Delta T}\varepsilon_L - \frac{1}{E}}$$

The radius R_1 is computed according to

$$R_1 = \frac{\beta\Delta T_{\varepsilon^{tr}}}{2}$$

Finally, R_0 has been assumed to be smaller than 50 MPa as it has been experimentally observed that a deformation due to

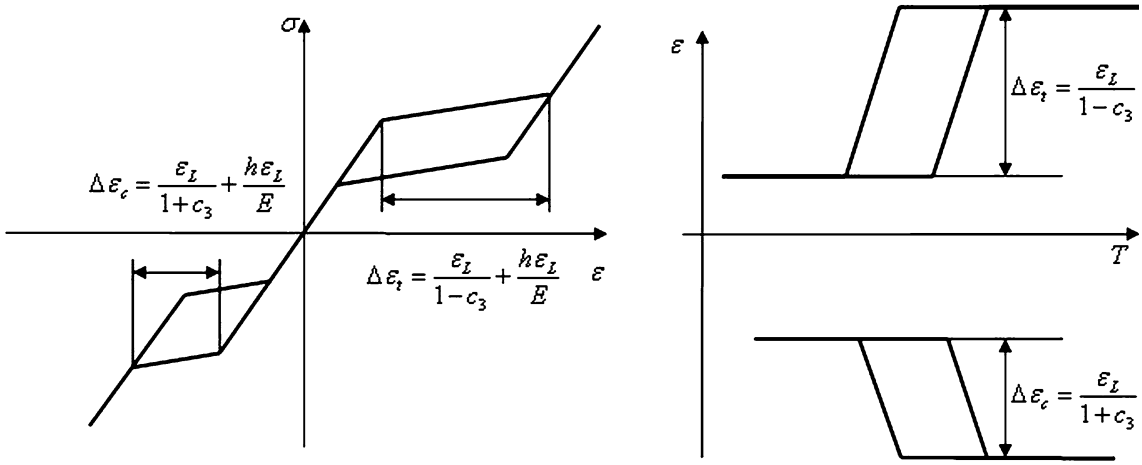

Fig. 4 Effect of the parameter c_3 in a typical stress-strain loop (left) and strain-temperature loop (right)

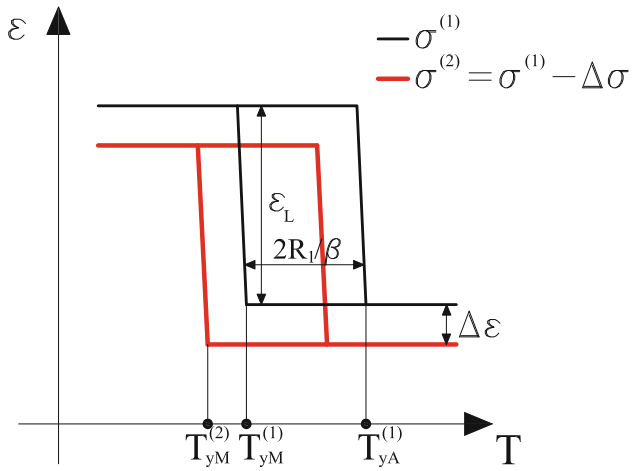

Fig. 5 Two strain-temperature curves at two constant stresses $\sigma_1 > \sigma_2$

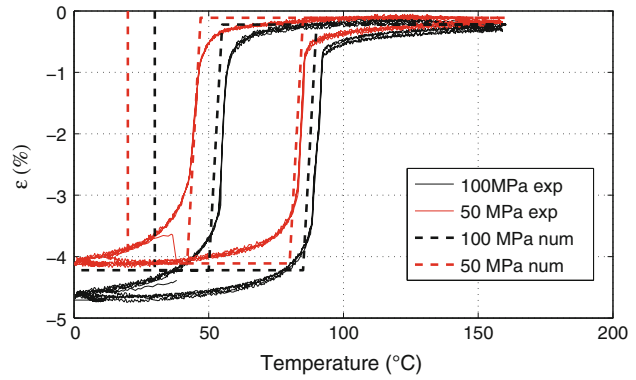

Fig. 6 Comparison of experimental and numerical curves at 100 and 50 MPa: the numerical curve at 100 MPa is fully fitted, while the one at 50 MPa is partially fitted and partially predicted

temperature induced transformation is present even at 50 MPa.

The following set of material parameters has been identified following the procedure described above:

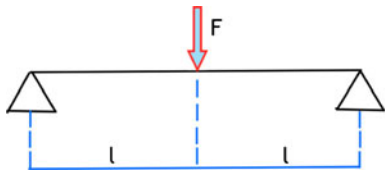

Fig. 7 Sketch of the bending testing conditions

$$E = 45\text{GPa},\ \frac{\varepsilon_L}{1-c_1} = 4.47\%,\ \beta = 5.22\,\text{MPa/K};$$
$$R_1 = 92\,\text{MPa},\ R_0 = 10\,\text{MPa},\ T^* = 57\,^\circ\text{C},\ h = 1000\,\text{MPa}.$$

The curve fitting can be appreciated in Fig. 6.

5. Behavior in Bending

A small deformation beam FE model (Ref 8), based on the standard Euler-Bernoulli theory (generally valid for thin beams and characterized by the hypothesis that plane sections normal to the beam axis remain plane and normal to the axis during deformation), has been implemented to compute the deformation of a beam during a temperature loop under a constant load in three-point bending configuration and to compare such numerical results with those from experimental tests. The considered geometry is sketched in Fig. 7: the pin to load distance has been fixed to be 0.5 mm, while the applied load is 0.65 N.

As far as experimental testing is concerned, temperature cycling at constant load in three-point bending conditions has been performed in a GABO Eplexor 150 N DMA. The following procedure has been followed: first, seven thermal cycles between −50 and 120 °C with a 0.65 N load have been performed in order to stabilize the material; then, one thermal cycle within the same temperature range has been performed at 0.65 N with a temperature rate of 1 °C/min. In Fig. 8, the numerical results obtained for different values of the parameter c_1 are compared with the last experimental loop only, to take into consideration just the stable material response.

From the reported diagrams, the effect of parameter c_1 on the beam displacement is clear: the displacement in the load application position decreases with increasing values of the

parameter c_1. This effect suggests the use of a bending test for the definition of c_1: in this case the best fit in terms of displacement is achieved with a value 0.4.

The start and finish temperature of the backward transformation and the start temperature of the forward transformation

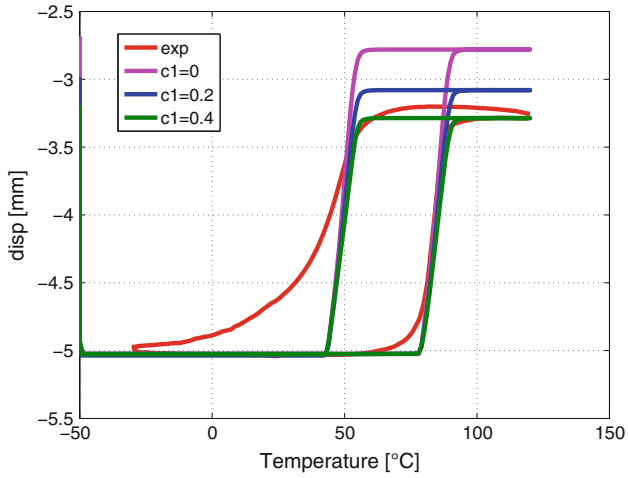

Fig. 8 Comparison of experimentally and numerically obtained curves in three-point bending for different values of the parameter c_1

in bending are well reproduced by the model. However, a discrepancy between the model and the experimental evolutions of the displacement is present in the final part of the forward transformation.

In order to appreciate the complex evolution of stresses and strains resulting from the solution of the bending problem, the stress and the transformation strain along the loaded cross section for different temperature conditions is investigated. In particular, we choose four significant points, highlighted in Fig. 9, corresponding to four different stress/transformation strain patterns in the section. These results are reported in Fig. 10 to 13, both for the case $c_1 = 0$ and $c_1 = 0.4$. It is noticeable how the section segment where the relevant transformation takes place is characterized by a flat region in the y-σ diagram. As the forward transformation proceeds, the mean stress of the plateau decreases from more than 100 MPa to less than 50 MPa.

6. Conclusions

In this study, we have considered a one-dimensional version of the phenomenological SMA constitutive model presented in Ref 3-5. Numerical results of three-point bending show how the computed load displacement depends upon the transformation

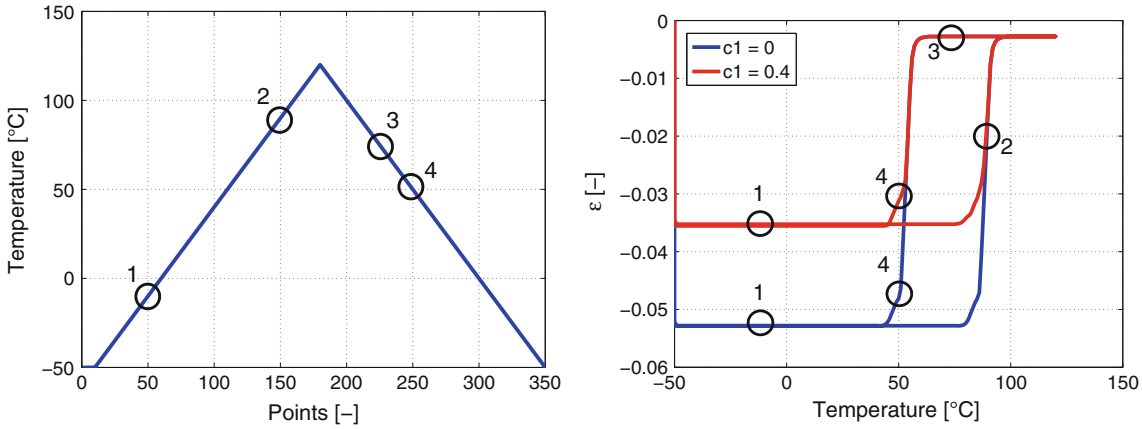

Fig. 9 Loading check-points for σ and ε^{tr} plots (cf. Fig. 10 to 13)

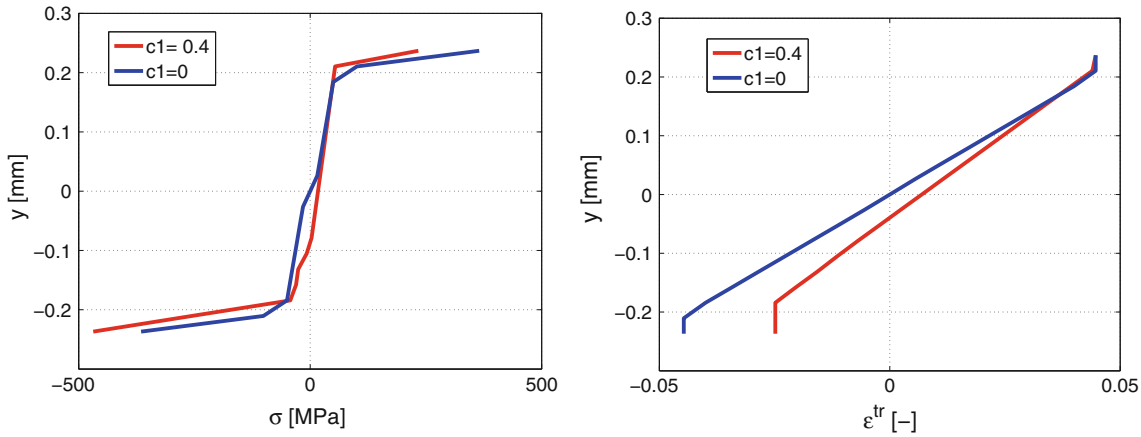

Fig. 10 σ and ε^{tr} in the loading section for point number 1 of Fig. 9

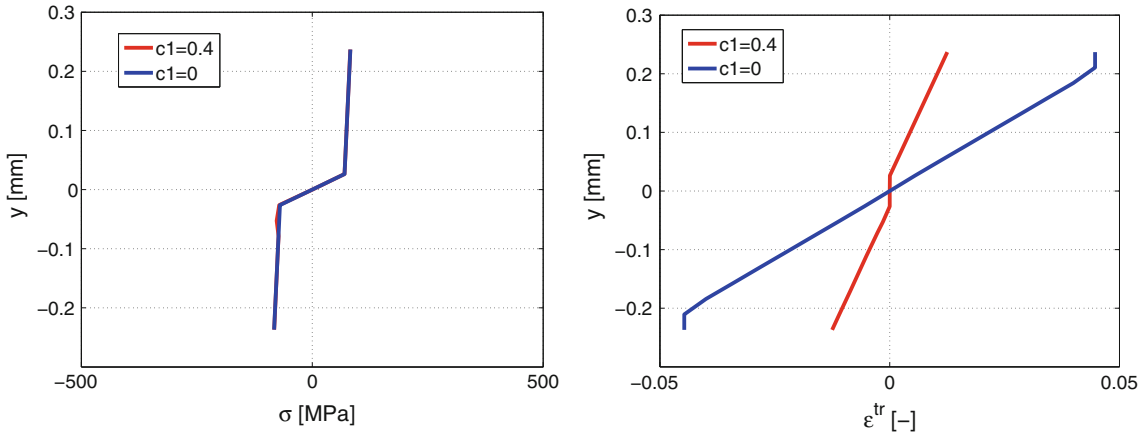

Fig. 11 σ and ε^{tr} in the loading section for point number 2 of Fig. 9

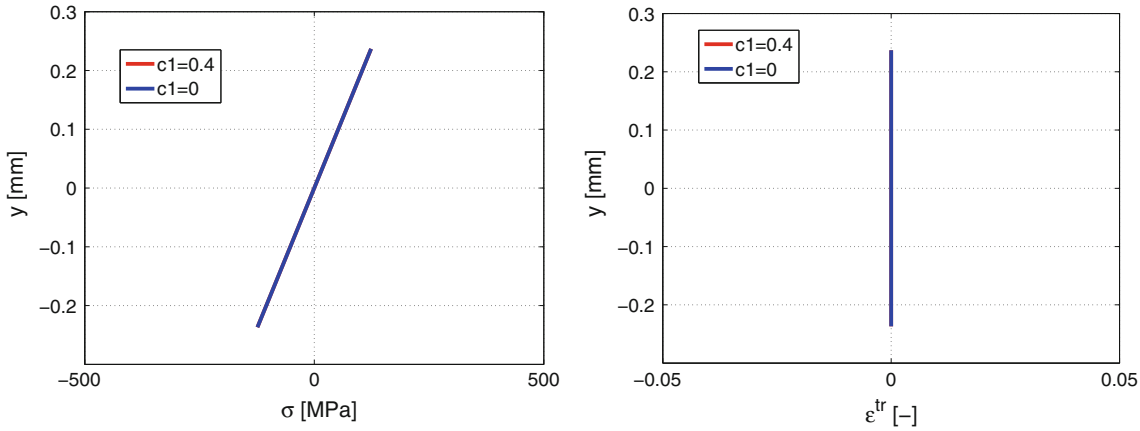

Fig. 12 σ and ε^{tr} in the loading section for point number 3 of Fig. 9

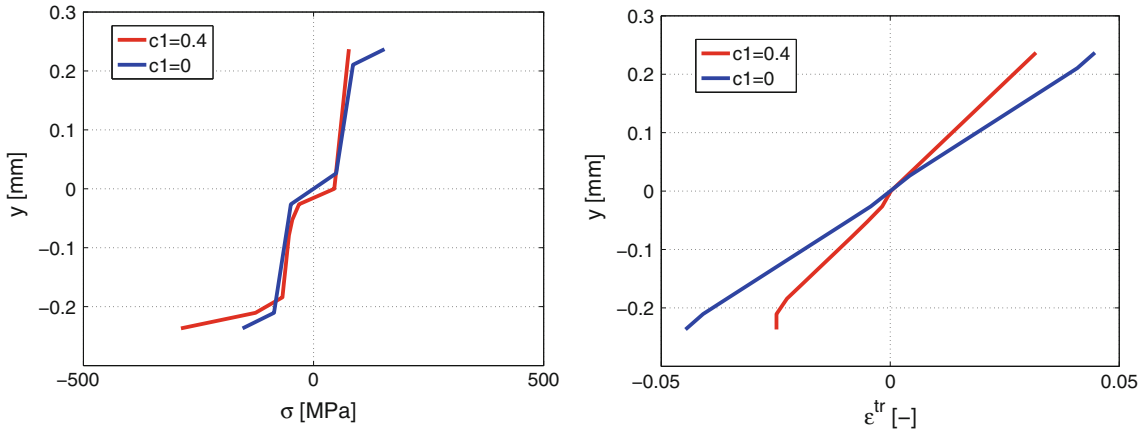

Fig. 13 σ and ε^{tr} in the loading section for point number 4 of Fig. 9

strain in compression. Fitting between numerical and experimental results of thermal cycling at constant load in bending allows for the identification of the transformation strain in compression. A comparison between experimental and numerical data evidences a good match between the start and the finish temperature of the backward transformation and the start temperature of the forward transformation. A discrepancy in the second part of the forward transformation is present. Investigation is ongoing to understand the reasons for such a discrepancy.

References

1. J. Arghavani, F. Auricchio, R. Naghdabadi, A. Reali, and S. Sohrabpour, A 3-D Phenomenological Constitutive Model For Shape Memory Alloys Under Multiaxial Loadings, *Int. J. Plast.*, doi:10.1016/j.ijplas.2009.12.003 (2009)
2. P. Sittner, L. Heller, J. Pilch, P. Sedlak, M. Frost, Y. Chemisky, A. Duval, B. Piotrowski, T. Ben Zineb, E. Patoor, F. Auricchio, S. Morganti, A. Reali, G. Rio, D. Favier, Y. Liu, E. Gibeau, C. Lexcellent, L. Boubakar, D. Hartl, S. Oehler, D.C. Lagoudas, and J. Van Humbeeck, Round Robin SMA Modelling, *Proceedings of ESOMAT*, Prague, 2009
3. F. Auricchio, A. Coda, A. Reali, and M. Urbano, SMA Numerical Modeling Versus Experimental Results: Parameter Identification And Model Prediction Capabilities, *J. Mater. Eng. Perform.*, 2009, **18**(5), p 649–654
4. F. Auricchio, A. Reali, and U. Stefanelli, A Macroscopic 1D Model for Shape Memory Alloys Including Asymmetric Behaviors and Transformation-Dependent Elastic Properties, *Comput. Methods Appl. Mech. Eng.*, 2009, **198**, p 1631–1637
5. F. Auricchio and L.A. Petrini, Three Dimensional Model Describing Stress Temperature Induced Solid Phase Transformation: Solution Algorithm and Boundary Value Problems, *Int. J. Numeric. Methods Eng.*, 2004, **61**, p 807–836
6. W. Huang, "Shape Memory Alloys and their Application to Actuators for Deployable Structures," Dissertation submitted to the University of Cambridge for the degree of Doctor of Philosophy, 1998
7. L.L. Toia, A. Coda, G. Vergani, L. Fumagalli, and F. Butera, Functional Characterization of SMA Wire in Actuation Conditions, *Proceedings of SMS*, 2006, p 499–506
8. O.C. Zienkiewicz and R.L. Taylor, *The Finite Element Method for Solid and Structural Mechanics*, Elsevier: Butterworth-Heinemann, Oxford, 2005